The fate of metal (Fe) during diesel combustion: Morphology, chemistry, and formation pathways of nanoparticles

Art Miller [a], Gib Ahlstrand [b], David Kittelson [c], Michael Zachariah [d]

[a] *NIOSH/Spokane Research Lab, Spokane, WA 99208, USA*
[b] *College of Biological Sciences, University of Minnesota, St. Paul, MN 55108, USA*
[c] *Department of Mechanical Engineering, University of Minnesota, Minneapolis, MN 55455, USA*
[d] *Department of Mechanical Engineering, University of Maryland, College Park, MD 20742, USA*

Abstract

This report describes an investigation in which we used iron-doped diesel fuel to generate metal-bearing diesel particles and a subsequent analysis of the particles using transmission electron microscopy (TEM) and energy-dispersive spectroscopy (EDS). For this study, DPM was generated by a 1.5-L diesel engine and the fuel was doped with ferrocene to enhance the level of iron in the system. The exhaust particles were collected on TEM grids and analyzed using the Philips CM12 TEM/EDS instrument. Results show that when the iron-to-carbon (soot) ratio (Fe/C) in the engine is low, the exhaust particles have morphologies similar to those for the undoped case, but at a threshold Fe/C value of 0.013 (for this engine), homogeneously nucleated metallic nanoparticles are formed and begin agglomerating. The number and size of these nanoparticles increase with level of doping. Metal-bearing particles that span a wider size range are also formed. Agglomeration of metallic and carbon particles is observed in two distinct modes: attachment of iron primary particles (5–10 nm in diameter) to carbon agglomerates, and coagulation of iron agglomerates (20–200 nm in diameter) with carbon agglomerates. Results of this work imply that as new engine technologies reduce soot levels in the engine and/or levels of trace metals in the fuel are increased, the generation of metallic nanoparticles may ensue, creating a potential health concern.

1. Introduction

Diesel engines produce a trimodal size distribution of diesel particulate matter (DPM) [1]. The newer "cleaner" engines, although they produce a smaller mass of particles, can sometimes produce a greater number of nanosized particles [2]. This "nuclei mode" of DPM is quite variable and can be attributed in many cases to the homogeneous or self-nucleation of volatile species during the dilution and simultaneous cooling of the exhaust aerosol as it exits the tailpipe [3]. It has also been shown that some nanoparticles may form prior to dilution and that this

phenomenon (early formation) can be enhanced by introducing trace amounts of metals into the fuel [4–6].

The dynamics of particle formation during and after combustion is a topic of much interest and investigation. A report summarizing the diesel combustion process [7] describes how the fuel jet quickly disintegrates as it exits the nozzle and vaporizes as it entrains hot air, subsequently forming a mixture plume of fuel vapor and air. It has been shown that soot precursors originate from partial oxidation of fuel in the fuel-rich region of this plume. It is postulated that within the plume, the high concentration of precursors interact to form soot primary particles that are quite spherical. Such particles begin to agglomerate and are mostly oxidized in the diffusion flame at temperatures around 2500 K, but some survive, presumably due to localized quenching and enter the combustion chamber. As combustion by-products exit the diffusion flame and as the piston subsequently moves downward, they undergo rapid cooling. During this cooling process, other nonvolatile gaseous species (such as metals) may begin to deposit onto the existing carbon particles. If the vapor concentration of such species is high enough, the rapid cooling may also drive their saturation ratios so high that they begin to self-nucleate, forming a new population of nanoparticles. The newly formed particles may then coagulate with existing particles as the aerosol travels through the exhaust system. Further cooling of the system en route to the tailpipe causes semivolatile species such as lube oil vapors and polycyclic aromatic hydrocarbons (PAHs) to condense onto the agglomerate particles. When the aerosol exits the tailpipe, it again cools rapidly and other more volatile species condense suddenly and/or self-nucleate into nanoparticles. The resulting complex mixture of particles is what we call DPM.

Both chronic and acute health effects have been shown to be associated with DPM, but the causal mechanisms are unclear. One theory suggests that the ultrafine and nanosized particles, i.e., particles less than about 100 nm in diameter, may play a key role in this association [8,9]. Although new techniques have been developed to characterize the size and morphology of such small particles, the issue of chemical composition and its links to particle formation scenarios is complex and remains elusive. The role of trace metals is of particular interest due to their possible toxicity [10,11] as well as their potential roles in atmospheric chemistry, and the research presented here thus focuses on the fate of metals in DPM, and their effects on particle morphology and chemistry.

Metals in diesel exhaust may originate from sources such as trace metals in the fuel [12] or from the use of metallic fuel additives for enhancing regeneration of diesel particulate filters [13], but under normal operating conditions most are believed to originate from lube oil additives and by-products of engine wear that enter the combustion chamber via reverse blow-by of the piston rings [14]. The research reported here provides insight into the role of such metals in the chemistry of DPM formation by investigating the formation of metal-rich nanoparticles via homogeneous nucleation and the overall distribution of metals across a wide range of particle sizes due to vapor deposition and coagulation.

The main goals of this work are to quantify the fate of a fuel-borne metal (Fe) during diesel combustion and to investigate how metal levels during combustion may affect the particle formation process. The research approach entailed using a diesel engine to generate exhaust particles and doping the fuel supply with ferrocene to introduce additional metal (Fe) into the combustion process, in amounts above the normal trace levels. For collecting data in the lab the engine was run and a sample of the exhaust was extracted and cooled/diluted. The aerosol was then routed to a suite of instruments (Fig. 1). The size distribution of the diesel aerosol was measured using a scanning mobility particle sizer (SMPS) and carbon levels in the exhaust were determined from filter samples using NIOSH method 5040 [15]. Particle samples were collected with a low-pressure impactor (LPI) or an electrostatic precipitator (ESP) and were analyzed using transmission electron microscopy (TEM) and energy dispersive spectroscopy (EDS).

2. Experimental setup and procedures

2.1. Experimental setup

The source of diesel particulate for this work was an Onan–Cummins “QuietDiesel” genset powered by a three-cylinder, 1.5-L Isuzu engine. This unit is capable of providing 10 kW of continuous ac power at a fuel flow rate of about 3 kg/h. In order to maintain a steady 60 Hz of ac current from the generator, the fuel flow to the engine is controlled by an electronic governor actuator that maintains a constant engine speed of 1800 rpm. The load on the engine is provided by a resistive load bank made by the Simplex Company. For the purposes of our experiments, the engine was run at conditions between 0 and 8 kW load. The corresponding fuel flow rates varied linearly from 1.1 to 2.6 kg/h. The fuel used for all tests was #2 diesel fuel with a nominal sulfur level of 350 ppm, doped with varying amounts of ferrocene to yield a fuel mixture containing from 20 to 600 ppm of iron.

During each test, the particulate matter for sampling/analysis was drawn isokinetically from the tailpipe, as shown in Fig. 1. The 3.8-cm-diameter exhaust line was connected to a fume hood system via

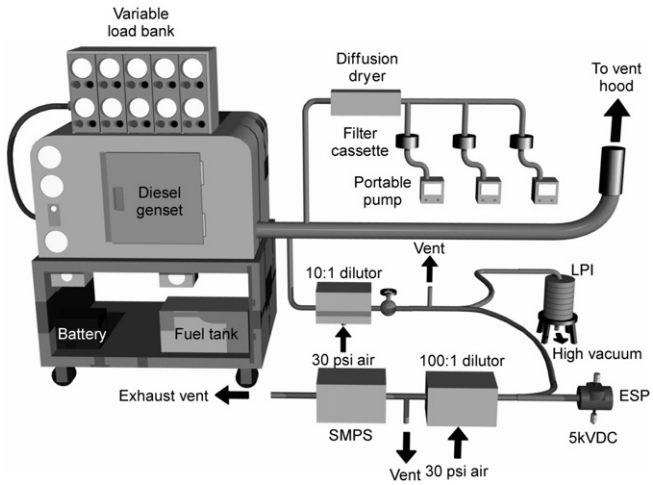

Fig. 1. Experimental setup.

a 10-cm-diameter pipe, and a 3-mm-ID stainless steel probe drew a small sample about 15 cm from the muffler exit. The probe was inserted through the tailpipe wall and directed into the exhaust stream. The opposite end of the probe was attached to the inlet of an AirVac TD260H vacuum pump that acted as an ejector dilutor [3]. The dilutor was fed a supply of 30 psi (200 kPa) dry air. Cold-flow calibration using a bubble flow meter at the dilutor inlet and a rotameter at the outlet yielded a dilution ratio of approximately 10:1 for this setup. For measurements of particle size distribution with the SMPS, the flow was further diluted as shown in Fig. 1. It should also be noted that the size distribution of particles generated by this engine varies somewhat from that of typical heavy-duty engines. Under normal operating conditions, which include a constant rpm of 1800, it produces no discernable nuclei mode and the accumulation mode decreases with engine load rather than increasing as it typically does for larger engines.

2.2. Particle sampling

Two methods were used to collect particles on TEM grids. The first method employed a low-pressure cascade impactor (LPI) to collect size-selected samples of particles larger than 50 nm (aerodynamic diameter). The second collection method employed an electrostatic precipitator (ESP), which does not yield a representative sample of particles due to charge biasing, but has the advantage of collecting a wide variety of particle sizes on one grid, including particles less than 50 nm (aerodynamic diameter). The samples were collected on 200 mesh copper TEM grids coated with either carbon (carbon-coated Formvar) or SiO films. The carbon films are more robust (therefore less damaged by the impactor jets) and, since they are thinner, yield better TEM images. The SiO films, since they contain no carbon, allow better EDS analysis of the carbonaceous particles.

The LPI is a simple method for classification of particles by aerodynamic size [16]. It consists of several sizing stages stacked on top of each other. The aerosol is drawn through the stack using a relatively low-pressure vacuum pump, which is where the LPI gets its name. The cascading stages are designed so that the aerosol sample is divided into predetermined size classes and impacted onto substrates, convenient for offline analyses of size-dependent particle characteristics. The LPI used in this work was designed to operate at −90 kPa outlet pressure and 1.0 lpm flow rate. For sample collection, cellophane tape was used to attach the TEM grids onto the impactor plates of the final three stages, i.e., stages 6, 7, and 8, which have design cut points of (Daero) 120, 75, and 50 nm, respectively.

The ESP used for these experiments was built in-house and is a simplified version of the Rochester design [17]. It consists of a brass tee plumbed so that the aerosol flows through the straight section. A small probe with a molybdenum platform is inserted into the tee connection with a TEM grid attached to the platform. The base end of the probe consists of a high-voltage coaxial fitting, wired so that the probe is at high voltage while the tee fitting is grounded. This design, unlike the point-to-plane (Rochester) design, does not generate a corona discharge and so depends on the intrinsic charge of particles to attract them onto the grid. For this reason its collection efficiency is much less, and the particles are collected with a charge bias. Despite these limitations, it provided a simple and effective way to collect a variety of particles from the aerosols sampled.

2.3. Particle imaging and analysis

Particles were imaged and photographed using a Philips CM12 TEM (FEI Company, Hillsboro, OR, USA) operating at 60 kV accelerating voltage and using TEM spot size settings of 2–5. Images were recorded on Kodak electron microscopy film 4489 and developed in Kodak developer D-19 at full strength for 3.0 min. Particles and nearby support substrate backgrounds (C and SiO films) were analyzed for elemental composition using a Power MX EDS system (EDAX, Inc., Mahwah, NJ, USA) fitted with a Super Ultra Thin Window X-ray detector (resolution 144.5 eV at Mn$K\alpha$ line, 40 μs time constant, 10 eV/channel, 45° takeoff angle). For EDS analysis, the TEM was operated at 60 kV, spot sizes 10–11, with objective aperture removed. Elemental ratios were calculated from spectra using the EDAX MX-TEM program "Materials Thin," which employs a thin-section approximation analysis strategy. When appropriate, substrate support film background spectra were subtracted from particle spectra.

3. Results and discussion

In this work we focus on the characterization of the nuclei and accumulation modes of DPM as defined previously [1]. Under normal operating conditions for this engine, the nuclei mode is absent and the accumulation mode consists of agglomerates of elemental carbon spheres, with hydrocarbons and other trace species condensed/adsorbed onto the surfaces of the agglomerates. When iron is added to the system in small quantities, it mainly attaches to particles via surface deposition [18]. At a certain threshold level of iron doping, vapor deposition cannot keep up with the locally high cooling rate and the supersaturation ratio of iron rises quickly. Homogeneously nucleated metallic nanoparticles are subsequently created and begin coagulating with each other and with other particles. These processes result in the evolution of distinct new particle morphologies, which are outlined and discussed below.

3.1. Identifying common particle morphologies

Five particle types were identified, representing the most common particle morphologies observed in samples. Each of the particle types is described below, including comments on the processes of condensation, nucleation, and coagulation as they relate to the fate of iron in the system. These processes may occur for other species as well, most notably for carbon, and the formation of carbon agglomerates is therefore covered first to provide a baseline for subsequent discussions of the interaction between metals and carbon in such a system.

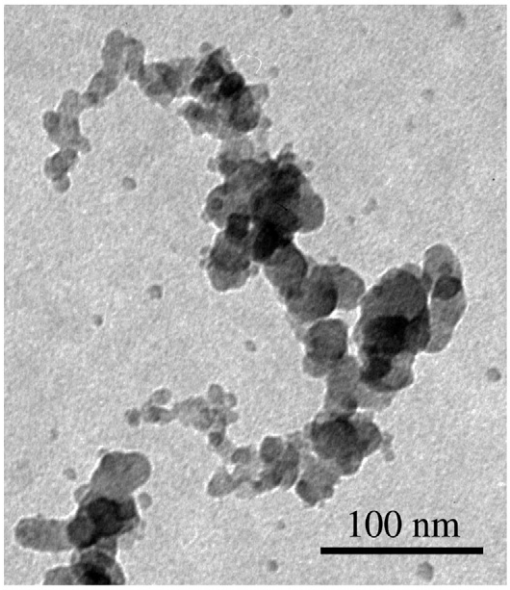

Fig. 2. Typical agglomerate of diesel soot (no metal doping).

3.1.1. "Type 1" particles: carbon agglomerates (accumulation mode of soot)

Under normal operating conditions, most particles are carbon agglomerates formed by coagulation of "spherules" of elemental carbon. The spherules are formed from soot precursors near the flame front, where temperatures are high and combustion chemistry dominates [19]. The extremely high concentration of free carbon and numerous collisions result in the formation of these 20–80 nm clusters of atoms and molecules consisting mainly of elemental carbon [20]. Due to the enhanced molecular mobility at high temperatures [20], these clusters arrange themselves into spherical shape and have been shown to have a layered structure [21]. These spherical particles are sometimes referred to as primary particles. The carbon agglomerates are subsequently formed when these primary particles begin to coagulate into larger chainlike agglomerates and eventually, as the system cools, take on other more volatile species by surface interactions.

For the undoped case, most observed particles are these "typical" carbon agglomerates (Fig. 2) with mean mobility diameter of around 80 nm. The mean diameter of the primary particles is approximately 20–30 nm, similar to that reported earlier [22]. Since the fuel is not doped, metal content is relatively low and virtually no "pure" metallic particles are observed. The trace metals in the system, derived from

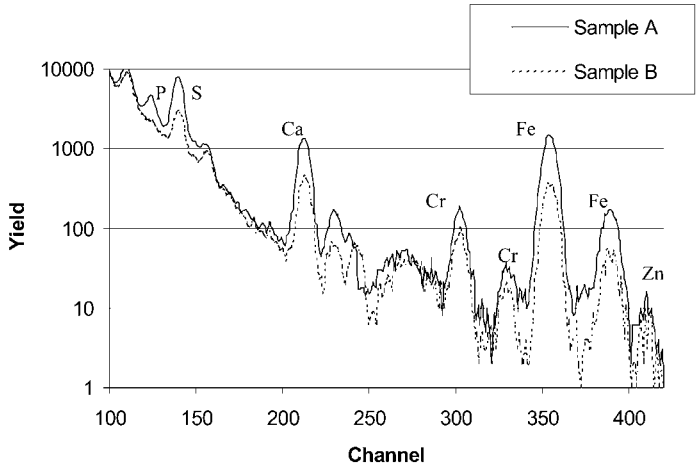

Fig. 3. PIXE data for Fe-doped case. Replicate samples A and B show presence of lube-oil additive metals (P, S, Ca, Zn) and engine wear metal (Cr).

fuel contaminants, lube oil additives, and engine wear, likely react in the gas phase to form metallic compounds [23], and as the system subsequently cools, they adsorb or condense relatively evenly onto carbon particles. For this undoped case the amount of metals residing on carbon particles is generally too low for detection using EDS. However, using particle-induced X-ray analysis (PIXE) on bulk samples of soot collected for the 20 ppm doping case (Fig. 3), we can detect that in addition to the iron, there are also other metals (fuel, oil, and engine-wear-related) present in smaller quantities. Others have done bulk analysis of diesel soot samples using inductively coupled plasma mass spectrometry (ICP-MS) with similar results [23].

3.1.2. "Type 2" particles: primary particles of metal (self-nucleated)

When the fuel is doped with just enough iron to trigger homogeneous nucleation, we see the appearance of a nuclei mode of small (<10 nm mobility diameter) metallic "primary particles" as evidenced by the beginnings of a nuclei mode for the 20-ppm doping case in Fig. 4. At and above this threshold condition, the amount of metal in the system is much higher than that for the undoped case, and the EDS technique can now be used to measure the metal on individual particles. For the lowest doping condition (20 ppm), EDS spectra from large particles show small amounts of Fe, but TEM images show no visibly dense regions indicating concentrated iron content. It is concluded that for this case the Fe on the particles is mainly from vapor deposition, with perhaps some coagulation of very fine nanoparticles or molecular clusters, and is thus not visible on the images. This was verified by our parallel study using single-particle mass spectrometry [18].

As the metal content in the system increases, more and larger self-nucleated metallic particles are generated. The primary particle size is initially less than 10 nm, as evidenced by both SMPS data (20-ppm case in Fig. 4), and TEM images such as in Fig. 5. Analysis of small particles such as those in Fig. 5 using EDS yields background levels of all species except Fe, suggesting they are composed mainly of iron. Note that the size of both primary particles and agglomerates appears to increase with increase in doping levels, especially notable for the 600-ppm doping case.

At lowest doping level (20 ppm), it is difficult to observe the primary iron particles using TEM. The SMPS data confirm their existence, and the shapes of particles such as those in Fig. 5a suggest that they coagulate into larger particles. However, they are so small that even when they coagulate into particles such as those in Fig. 5a, it is not possible to resolve the primary particles with our TEM. At higher doping rates, the primary iron particles are larger and we are then able to resolve the individual primary particles.

The potential role of iron oxide primary particles that may form early in the combustion process, perhaps even in the core of the diffusion flame as described in an earlier work [24], is unclear. For premixed flames [25,26], addition of ferrocene was shown to trigger the homogeneous nucleation of iron oxide nanoparticles, which formed prior to the soot, and in fact reportedly enhanced soot production, since their high surface reactivity encouraged soot deposition. These soot particles were described as then being immune from surface oxidation as they passed through the remainder of the flame, since the metal could not diffuse through the carbon and reach the

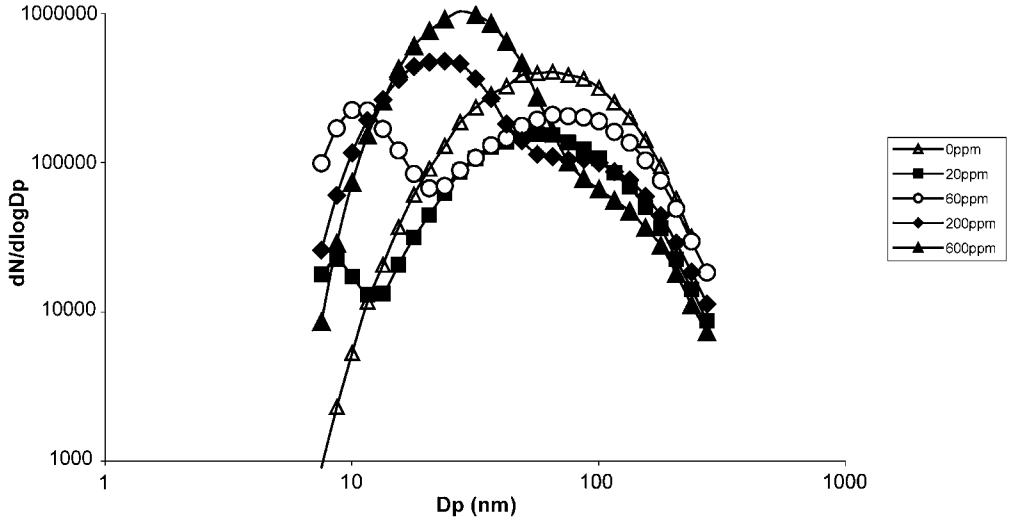

Fig. 4. Effect of iron doping level on the size distribution of diesel particles. Engine load of 0 kW and dilution of approximately 700:1 for all cases.

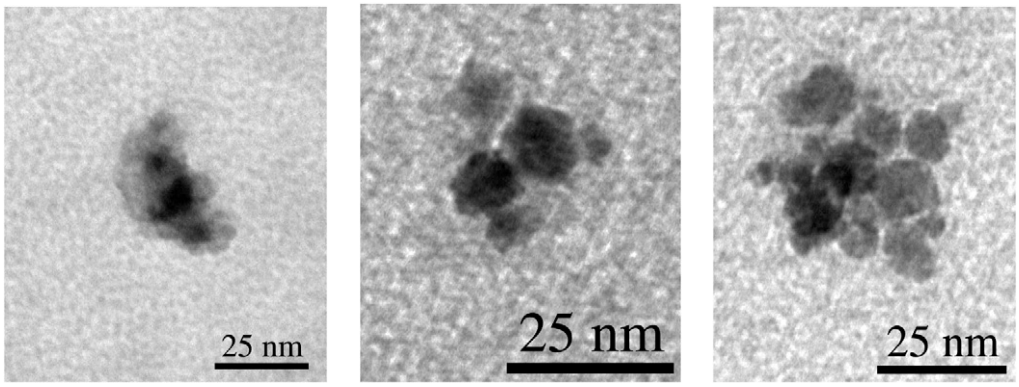

(a) (b) (c)

Fig. 5. Iron agglomerate nanoparticles showing primary particle size and typical agglomerate diameters for three doping conditions: (a) 60 ppm, (b) 200 ppm, (c) 600 ppm.

surface fast enough. On the other hand, laminar diffusion flames [24] have been shown to display the same behavior, i.e., early generation of metal oxide nanoparticles, but (perhaps due to reduced oxygen availability) this process appeared to be limited, leaving sufficient metal in the system to form metal oxide coatings on the soot particles, evidenced by their high rate of oxidation later in the flame. Neither of these studies indicated that metal played a role in suppression of soot during the combustion process. However, a later study [27], in which soot concentration was measured in the cylinder as a function of crank angle, suggested not only that during diesel combustion of metal-doped fuel, soot oxidation is enhanced due to its metallic surface film, but also that its formation is suppressed. The validity of that approach may be in question, however, since the soot measurements were not taken inside the diffusion flame, but rather in the prechamber, i.e., where the flame initiated.

The creation of iron oxide particles during diesel combustion with 200 ppm Fe doping is suggested by EDS data such as in Fig. 6, which shows a distinct oxygen peak for a 78-nm metallic agglomerate. However, analysis of the relative mole fractions of iron and oxygen on a number of such particles did not yield consistent stoichiometric ratios commensurate with any particular FeOx compounds. It is also possible that the self-nucleated metallic particles are pure iron and that they oxidize en route to the TEM. This is supported by the lack of O peaks in the single-particle mass spectra in our previous work [18]. Since the boiling point of iron is high, it is possible that the Fe primary particles form only after Fe passes through the diffusion flame. In that case, the local

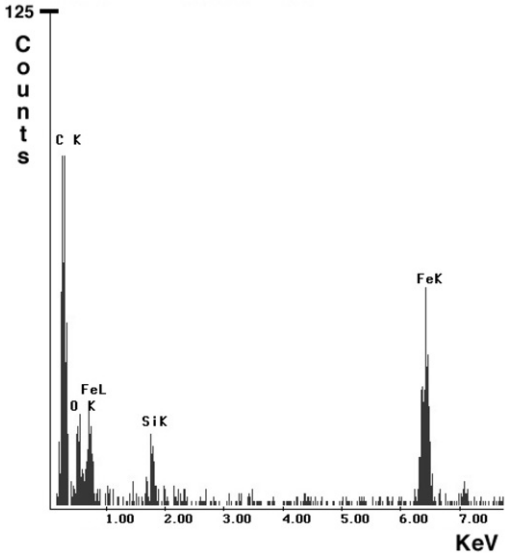

Fig. 6. EDS spectrum of metallic nanoparticle showing iron and oxygen.

reducing environment of CO would limit the formation of oxides, which would explain our observation of "pure" iron nanoparticles. We therefore conclude that most observed nanoparticles are pure iron particles that self-nucleate after iron is vaporized in the diffusion flame and subsequently cool in the reducing environment outside the flame. It is hypothesized that such primary particles subsequently coagulate to a self-preserving size distribution, which is in fact the lognormal distribution making up the nuclei mode for the doped cases.

3.1.3. "Type 3" particles: carbon agglomerates decorated with iron nanoparticles

Before or during the mutual coagulation of the primary iron particles, they also individually collide with carbon agglomerates and "decorate" the agglomerate surfaces with "nanonuggets" of relatively pure iron. This is confirmed by observation of very small nuggets of dense material visible on TEM images of carbon agglomerates (Figs. 7a–7b). The dense nuggets are assumed to be self-nucleated primary particles of iron attached directly to carbon surfaces. This process is also documented for the case of Ce-doped diesel combustion [13]. This decorating of carbon agglomerates may also explain the observation of minute dark specks on some carbon agglomerates at lower doping levels. For such cases, the size of the primary iron particles is potentially so small that they are not easily resolved in the TEM images, but rather appear as tiny specks (Fig. 7c). Note that for Figs. 7 and 8, since the number and size of iron nuggets correlate with iron availability, the mass flow rate of Fe is used instead of simply the doping level.

3.1.4. "Type 4" particles: metal agglomerates

After homogeneous nucleation of iron is established, further increase in metal above the threshold level simply creates more (and slightly larger) primary particles. Large numbers of such monodisperse particles drive coagulation and this creates the growing "nuclei mode" of metallic (agglomerate) particles we see in Fig. 4. The mean diameter of this nuclei mode of metal agglomerates depends on the quantity of metal available. For example, at 600 ppm doping (Fig. 4), the mean mobility diameter of such agglomerates increases to approximately 30 nm (see Fig. 5c, which is typical of such particles).

The fact that the growing nuclei mode is a direct result of metal nucleation and agglomeration is shown in Fig. 8. The linear growth of particulate volume (mass) in the nuclei mode corresponds directly to the increase in mass flow rate of Fe through the system. For this figure the nuclei mode volumes were calculated from SMPS size distributions and the Fe flow rates were calculated as the product of fuel flow rate and doping level. For the conditions of our tests, the "threshold" Fe flow rate for the onset of homogeneous nucleation is at about 0.025 g/h, i.e., where the trend line crosses the x-axis in Fig. 8. This value corresponds to the product of fuel flow rate at 0-kW load (1.1 kg/h) and approximately 23 ppm Fe doping of the fuel. Since the threshold is also affected by the availability of carbon surfaces for metal deposition, we use this threshold Fe flow rate along with the (baseline/undoped) carbon mass measurements presented later in section C to calculate a threshold iron-to-carbon ratio of 0.013 for onset of homogeneous nucleation for this case. In Fig. 9 we show that the calculated Fe/C ratios for all loads are well above this threshold for the 60-ppm doping case, which is supported by experimental results, while the Fe/C ratio at 0 kW and 20 ppm doping is near the threshold of nucleation. The latter was observed experimentally and is reflected in Fig. 4. Note that due to the wide range of metal-to-carbon ratios used to derive the trend line, the Fe/C ratio at 0 kW actually appears slightly below the threshold in Fig. 9, while the existence of a nuclei mode for the 20-ppm case in Fig. 4 confirms that it is in fact above the threshold.

As metal levels increase, further coagulation of metallic particles leads to the formation of larger metal agglomerates. This is evidenced by observation of ~100-nm "pure" iron particles in the single-particle mass spectra for the case of 60 ppm doping [18]. For the lowest doping rate (20 ppm), such particles are virtually nonexistent, but for the highest doping rate (600 ppm), they are fairly common.

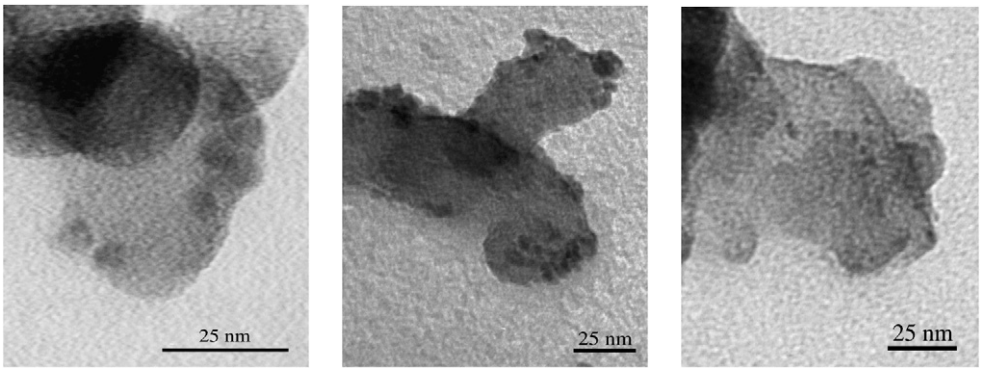

(a) (b) (c)

Fig. 7. TEM images showing metallic primary particles, the darker spots/specks that decorate lighter-colored carbon agglomerates at Fe flow rates of (a) 0.158 g/h, (b) 0.115 g/h, and (c) 0.063 g/h.

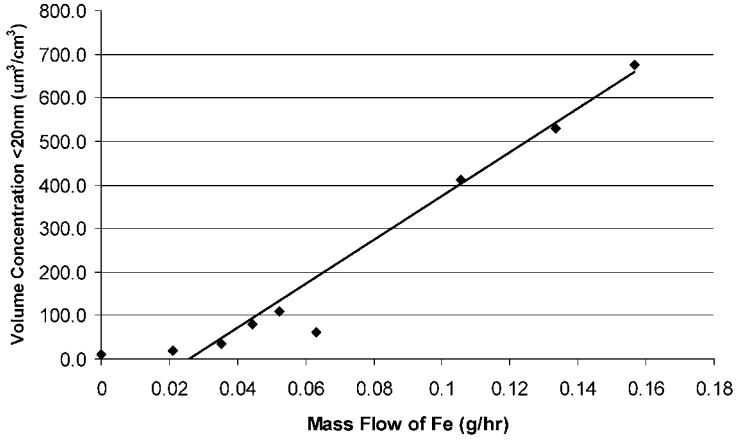

Fig. 8. Volume of nuclei mode particles (<20 nm) as a function of Fe throughput.

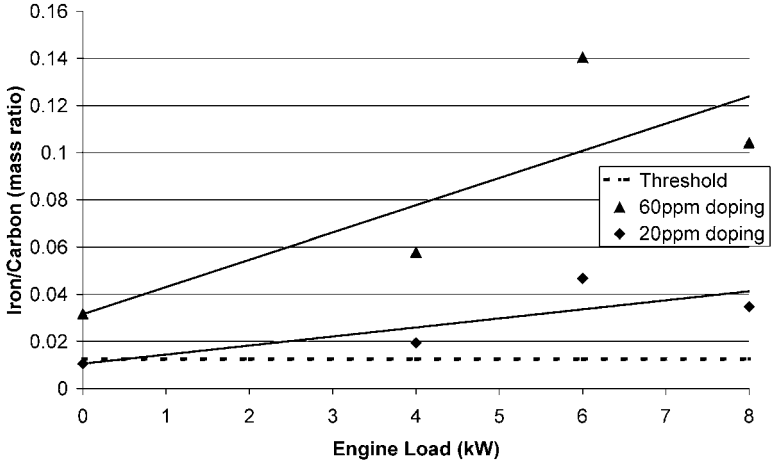

Fig. 9. Data showing variation in iron-to-carbon ratio with doping level and engine load.

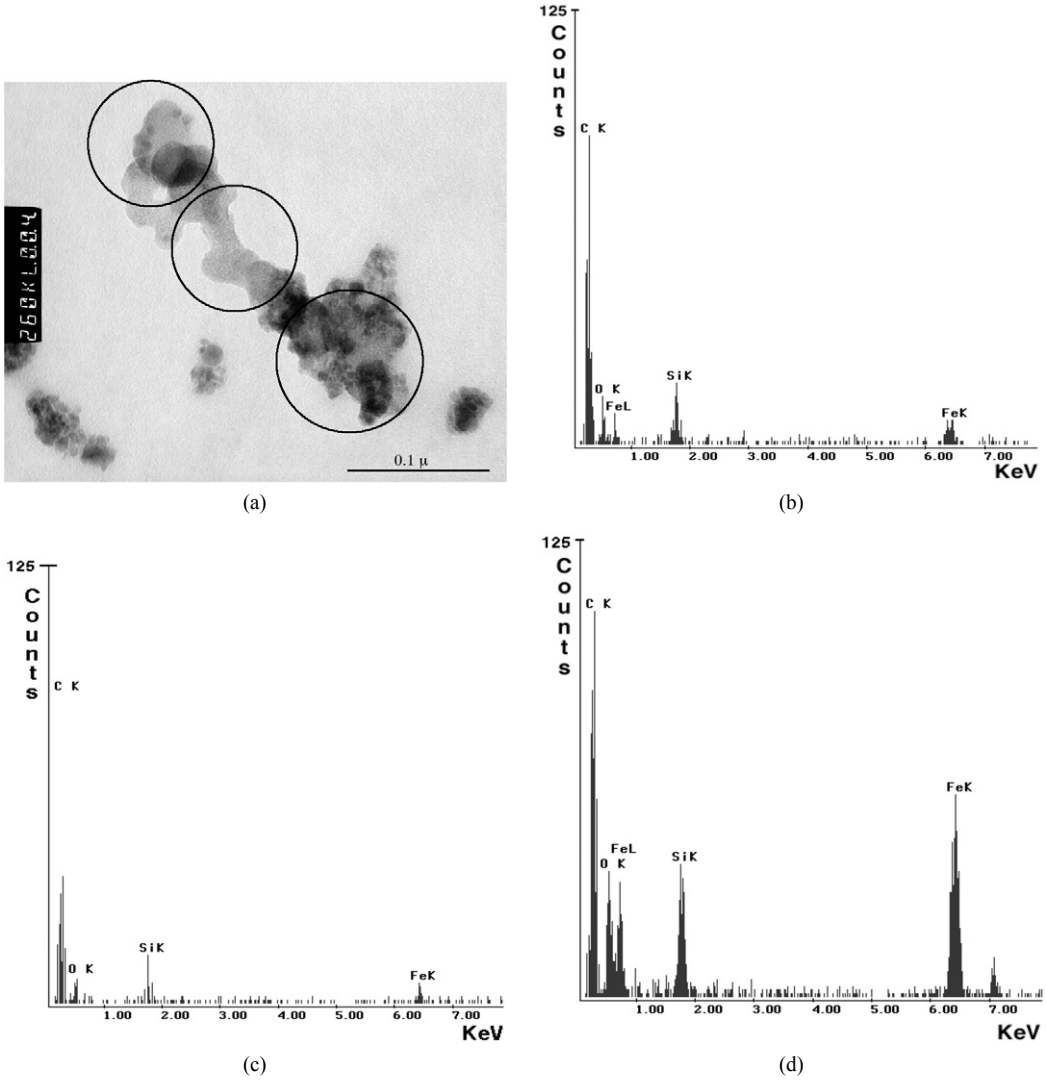

Fig. 10. TEM image and EDS spectra show how iron content is related to morphology. (a) Image of combination iron–carbon particle. (b) EDS spectrum for upper end of particle. (c) Spectrum for midsection. (d) Spectrum for lower section.

3.1.5. "Type 5" particles: combined metal/carbon agglomerates

For iron doping levels at and above 60 ppm, we observe large agglomerate particles that contain significant amounts of both iron and carbon. An example of such a particle is shown in Fig. 10a. Three consecutive localized EDS scans of this particle (Figs. 10b–10d) show clearly the association between morphology and chemistry. The upper end of this particle consists of a carbon agglomerate structure with a few very small metallic primary particles visible, and the spectrum of Fig. 10b shows a relatively small iron peak for this case. The spectrum of Fig. 10c shows an even smaller iron peak for the low-density (carbonaceous) central portion of that particle. Finally, Fig. 10d shows a very large iron peak, suggesting that this end of the particle was formed by coagulation with a type-4 metallic agglomerate.

Fig. 10a thus demonstrates the two different modes of coagulation for metallic and carbon species that may take place during the complex particle formation process. First, the very small iron primary particles visible on the upper left end of the chain show how self-nucleated particles attach directly to carbon surfaces. Second, the structure on the lower right indicates coagulation of larger metallic agglomerates with carbon particles, an observation supported by single-particle mass spectrometry [18]. Both these processes are collision-driven and so will increase in

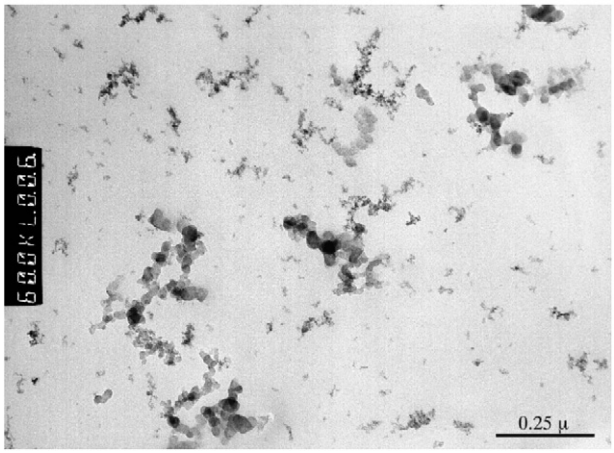

Fig. 11. Sample taken with ESP shows the great variety in particle morphologies for the case of 60 ppm Fe doping of fuel.

frequency as the metal in the system and thus the concentration of metallic particles increases.

Fig. 11 further demonstrates the variation in particle size, morphology, and elemental composition for the metal-bearing exhaust aerosol. This sample was collected from raw exhaust (using 60 ppm Fe doping) with an electrostatic precipitator. This collection method favors highly charged particles, so the sample is not necessarily representative, but it does clearly show the variation in particle morphologies that occur at these doping levels. Note that the agglomerates with larger primary particles were shown to be carbonaceous, while those with smaller (and more dark/dense) primary particles were rich in iron.

3.2. Relative frequency of particle types as a function of metal throughput

The five particle types described above appear with varying frequencies depending on doping level. This is best visualized by comparing TEM images of particles collected on the eighth stage of the LPI at different doping levels (Figs. 12–15). Note that the particle number density in the photos is not necessarily representative, due to variable loading of the TEM grids. In the following descriptions, references to iron content were verified by EDS analysis.

At the highest doping condition of 600 ppm (Fig. 12), "pure" type-1 carbon particles do not exist, while there are numerous type-4 metal agglomerate particles and type-5 combined particles. This is the only condition at which the large type-4 metal agglomerates are readily found, and we also see considerable numbers of type-3 Fe-decorated carbon particles. For the latter, the Fe appears as tiny dots on the larger carbon particles, as seen in Fig. 12b.

Fig. 13 shows that at the next lower doping level (200 ppm), the type-4 metal agglomerate particles are still prevalent. The type-5 combined particles are now less prevalent, and the number of primary metal particles attached directly to carbon agglomerates is also reduced (Fig. 13b).

At the 60-ppm doping level (Fig. 14), the type-4 metal agglomerate particles are still fairly prevalent. The type-1 carbon agglomerates are plentiful, while type-5 particles are now infrequent. Direct attachment of primary metal particles to carbon agglomerates is still evident but infrequent, and since the primary particles are very small, they are sometimes hard to resolve on TEM images such as in Fig. 14b.

At the lowest doping level (20 ppm), the type-5 particles are gone and the type-4 particles are rare (Fig. 15). Since few if any type-2 particles exist, the nanoparticles observed in these images are carbonaceous (this was confirmed using EDS). Under this condition, most of the particles are type-1 particles. These particles contain small amounts of iron but their appearance is similar to the undoped particles of Fig. 2. A potential exception to that similarity is the possibility of greater variation in primary particle size for the 20-ppm doped particles.

This disparity in the size of primary carbon particles could be due to enhanced postcombustion oxidation of the doped particles as they make their way through the exhaust system. For the case of no doping the carbon primary particles have a fairly narrow lognormal distribution in size [22]. Since the relative amount of vapor deposition of both metallic and hydrocarbon species would favor smaller particles due to their high surface-to-volume ratio, these particles are likely to oxidize faster than their larger neighbors, leading to the skewed size distribution (greater number of smaller particles) observed in Fig. 15, as compared to Fig. 2. Further work should be done to confirm this statistically.

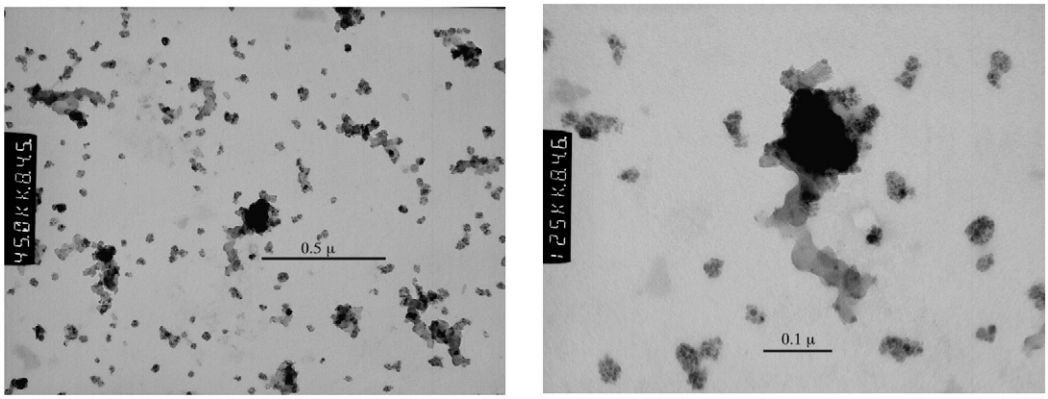

(a) (b)

Fig. 12. (a) LPI stage 8 sample, 600-ppm doping rate, 0 kW engine load, showing prevalence of iron agglomerates (type 3) and combination iron/carbon particles. (b) Zoom of same shows primary iron nanoparticles (type 2) decorating a carbon agglomerate.

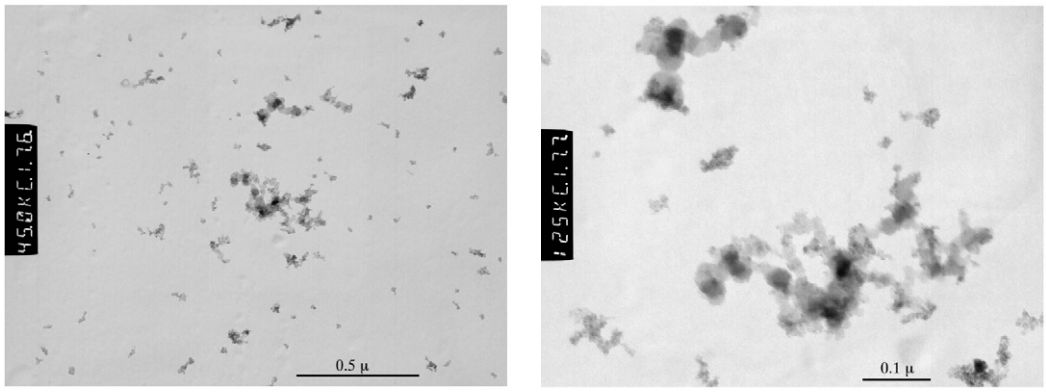

(a) (b)

Fig. 13. (a) LPI stage 8 sample, 200 ppm doping, 6 kW load. (b) Zoom of same showing small iron agglomerates and iron nanoparticles decorating a carbon agglomerate.

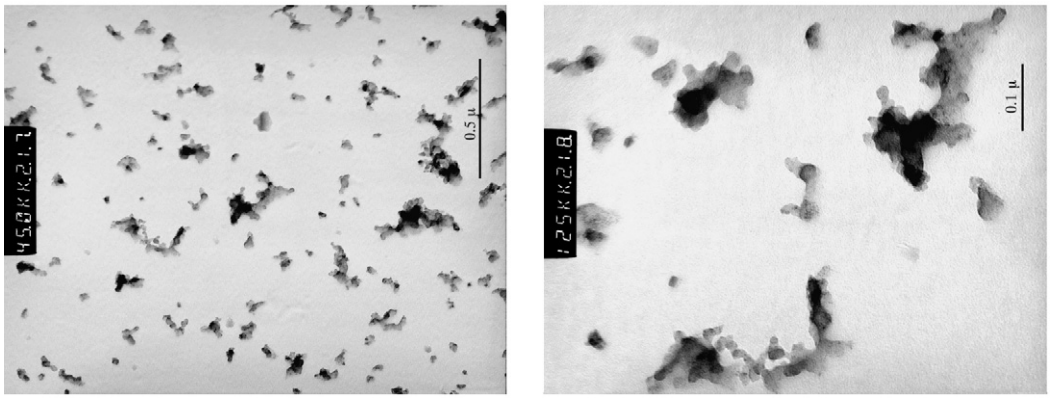

(a) (b)

Fig. 14. (a) LPI stage 8 sample, 60 ppm doping, 6 kW load. (b) Zoom of same showing small metal agglomerates and very fine iron nanoparticles decorating a carbon agglomerate (upper right corner).

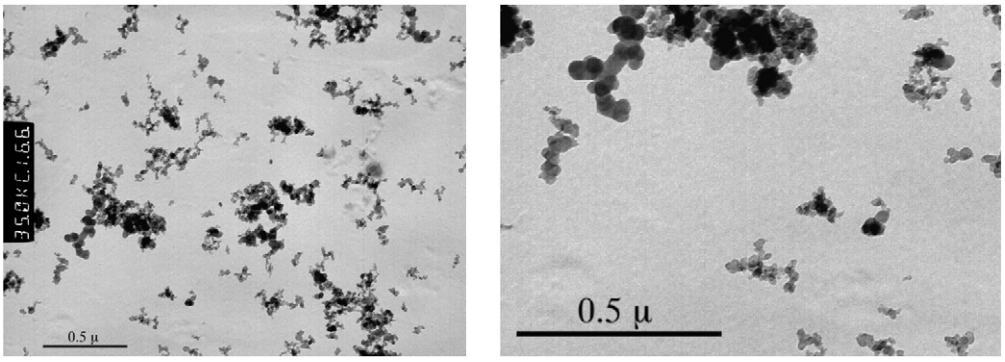

(a) (b)

Fig. 15. (a) LPI stage 8 sample, 20 ppm doping, 6 kW load. (b) Zoom of same showing carbonaceous agglomerates and nanoparticles, as well as variation in size of carbon primary particles.

3.3. Metal enhanced decrease in soot production

The addition of ppm levels of metals to diesel fuel has been shown to decrease soot emissions [4]. We confirmed this result for the case of 60 ppm iron doping by using the NIOSH Standard Method 5040 [15] to measure elemental carbon (EC) and organic carbon (OC) in the raw exhaust. In Fig. 16 we compare the baseline (undoped) values of total carbon (TC = EC + OC) with the case for the doped condition. Decreases in total carbon are on the order of 20–40%, which is commensurate with metal-induced decreases in soot production reported earlier [13].

Using the NIOSH method 5040 allows us to look separately at metal-induced decreases in EC and OC. Notably, OC is decreased significantly and in fact accounts for most of the decrease in total carbon. Fig. 17 shows OC decreases on the order of 65–85% for the three engine loads tested.

The trend of decreasing total carbon with engine load is also reflected in Fig. 4, which indicate a decrease in accumulation mode particles for higher doping. Similarly, the data of Fig. 17 suggest greater relative reductions in total carbon at higher engine load. Although those data are for 60 ppm doping only, the absolute throughput of iron increases about 2.5 times between the lower and higher engine load conditions due to increased fuel flow, and the added iron may account for the enhanced decrease in carbon (due to metal-enhanced oxidation) indicated by the data.

3.4. Formation pathways for metal-bearing particles

Based on the results of our study, the following is a description of plausible formation pathways for the resulting particles.

Using the assumption of a quasi-steady-state combustion process [7], the ferrocene-doped fuel exits the injection nozzle at high velocity and forms a plume

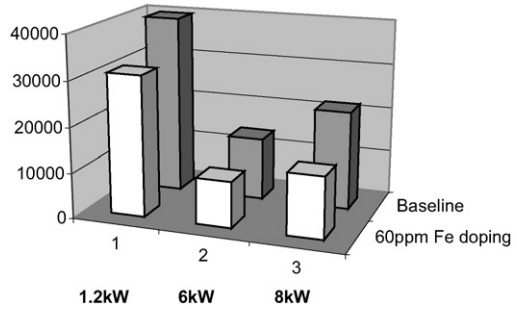

Fig. 16. Comparison of total carbon (TC) measurements with and without 60 ppm Fe doping.

of fuel vapors with a diffusion flame at its periphery (Fig. 18). The plume entrains hot air and temperatures inside reach about 1600 K. Since the ferrocene decomposes at around 750 K [4], it is expected that as the fuel droplets vaporize, the ferrocene also vaporizes. Subsequent thermal decomposition of ferrocene vapor would then lead to the existence of iron vapor at or near the hotter (∼2500 K) flame front, creating the conditions for vapor deposition and/or homogeneous nucleation of iron particles just outside the flame front.

Iron vapor derived from the ferrocene experiences sudden cooling as it leaves the flame front and again as the piston retracts (Fig. 19). The cooling raises the saturation ratio of iron, and vapor begins adsorbing and condensing onto existing particle surfaces. If the amount of iron vapor is high compared to available surface area (mainly carbon agglomerates), condensation cannot convert the vapors fast enough (since it is rate-limited) and the saturation ratio rises quickly, triggering homogeneous nucleation of primary particles. The absolute amount of a given species, in this case iron, along with local temperature and cooling rate, would determine the extent of these processes and thus affect the size of the homogeneously nucle-

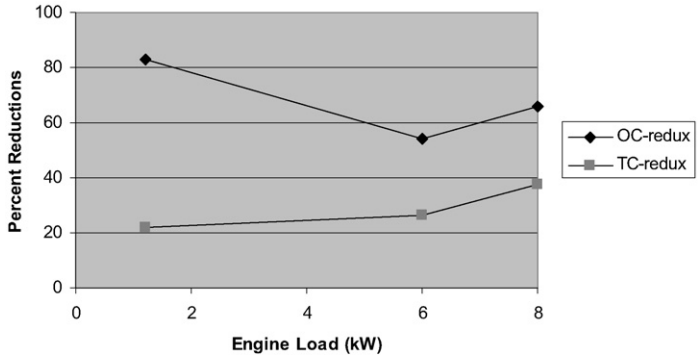

Fig. 17. Reductions of total carbon (TC) and organic carbon (OC) with engine load for the case of 60 ppm Fe doping of fuel.

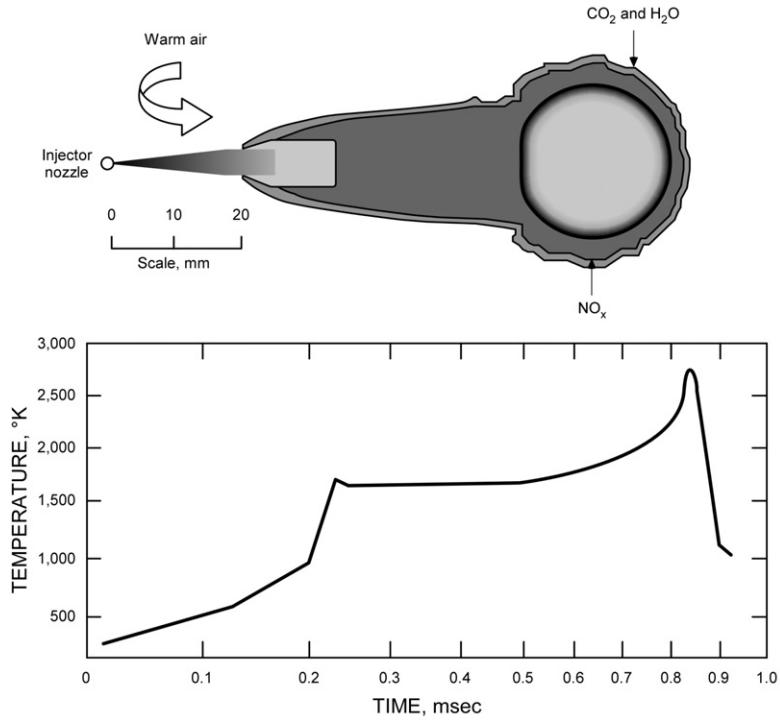

Fig. 18. Depiction of the diesel combustion process after Flynn et al. [7].

ated particles. During and after formation of these primary particles of iron, they coagulate with each other and with larger carbon agglomerates, leading to the five particle types described above.

The presence of iron in the system leads to measurable decreases in soot production. There are two probable causes for this:

(1) The first is the suppression of soot inside the diffusion flame. This was suggested in earlier work [27], but a definite mechanism was not identified. It could possibly result from iron vapors, thermally decomposed from ferrocene, interacting with free carbon and/or local soot precursors (carbon fragments) and catalyzing their destruction. Our data were inconclusive in this regard.

(2) The second cause is the iron-accelerated oxidation of carbon in the cooler region outside the flame (and after the flame goes out). This would include both gas-phase reactions and the (later) oxidation of organic compounds attached to the surfaces of carbon agglomerates. The plausibility of the latter has been demonstrated in earlier work [13] and is supported by the data of Fig. 17.

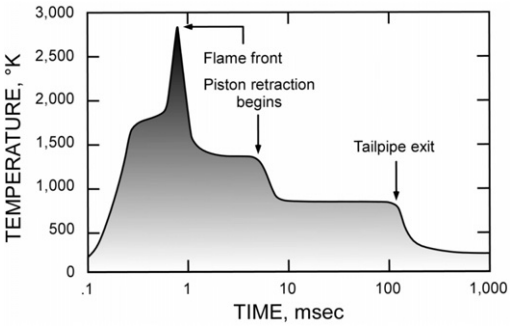

Fig. 19. Temperature history during typical diesel combustion.

4. Conclusions

Using ferrocene doping of diesel fuel, we have shown that for this diesel engine, when the iron-to-carbon (soot) ratio is above a threshold of approximately 0.013, iron nanoparticles form during combustion and subsequently coagulate with each other as well as with larger carbon agglomerates.

At conditions below this threshold, emitted particles will have relatively uniform morphology and elemental chemistry, consistent with agglomeration of carbon spheres followed by adsorption and condensation of other species onto the agglomerate surfaces. Above the threshold, five distinct morphologies are identifiable: (1) carbon agglomerates, (2) homogeneously nucleated primary particles of iron, (3) carbon agglomerates decorated with these iron primary particles, (4) agglomerates of the iron primary particles, and (5) combined agglomerates of iron and carbon. Plausible formation pathways were presented, based on the (combustion) temperature history in a diesel engine, and supported by data showing change in size, morphology, and iron content as doping levels were increased.

The demonstrated fact that metallic nanoparticles will form at a threshold metal-to-carbon ratio has important implications. It suggests that as engine combustion technologies improve, the “cleaner” engines, i.e., those that generate less soot, will be more likely to generate metallic nanoparticles. The source of metals for such particle generation could be from fuel impurities, lube oil consumption (lube oil often contains some metal additives), or metals derived from engine wear. Due to their small size and thus efficient lung penetration, the generation of such metallic nanoparticles could introduce a new health concern.

References

[1] D. Kittelson, J. Aerosol Sci. 29 (1998) 575–588.

[2] L.D. Gratz, S.T. Bagley, D.G. Leddy, G.M. Pataky, K.J. Baumgard, J.H. Johnson, Prepr. Am. Chem. Soc. Div. Pet. Chem. 37 (4) (1992) 1430–1436.

[3] I. Abdul-Khalek, D. Kittelson, B.R. Graskow, Q. Wei, F. Brear, Paper 980525, Society of Automotive Engineers, 1998.

[4] C.J. Du, J. Kracklauer, D. Kittelson, Tech. Paper 980536, Society of Automotive Engineers, 1998, pp. 1–13.

[5] D. Kittelson, I. Abdul-Khalek, Y. Chwen, C. Du, D. Haugen, E. Stenerson, Paper 941015, Society of Automotive Engineers, 1994.

[6] G. Skillas, Z. Qian, U. Baltensperger, U. Matter, H. Burtscher, Combust. Sci. Technol. 154 (1) (2000) 259–273.

[7] P. Flynn, R. Durrett, G. Hunter, A. Loye, O.C. Akinyemi, J. Dec, C. Westbrook, Tech. Paper 1999-01-0509, Society of Automotive Engineers, 1999, pp. 1–14.

[8] M.J. Utell, M.W. Frampton, J. Aerosol Med. 13 (2000) 355–359.

[9] C.A. Pope III, M.J. Thun, M.M. Namboodiri, D.W. Dockery, J.S. Evans, F.E. Speizer, C.W. Heath Jr., Am. J. Resp. Crit. Care Med. 151 (1995) 669–674.

[10] A.G. Ghio, J.H. Richards, J.D. Carter, M.C. Madden, Toxicol. Pathol. 28 (4) (2000) 619–627.

[11] A.E. Aust, J.C. Ball, A.A. Hu, J.S. Lighty, K.R. Smith, A.M. Straccia, J.M. Veranth, W.C. Young, Research Report 110, Health Effects Institute, 2002, pp. 67–76.

[12] Y.F. Wang, K.L. Huang, C.T. Li, H.H. Mi, J.H. Luo, P.J. Tsai, Atmos. Environ. 37 (2003) 4637–4643.

[13] H. Jung, D.B. Kittelson, M.R. Zachariah, Combust. Flame 142 (3) (2005) 276–288.

[14] C. De Petris, V. Giglio, G. Police, Tech. Paper 961216, Society of Automotive Engineers, 1996.

[15] M.E. Birch, Appl. Occup. Environ. Hygiene 17 (6) (2002) 400–405.

[16] S.K. Hering, S.K. Friedlander, J.J. Collins, L.W. Richards, Environ. Sci. Technol. 13 (2) (1979).

[17] Y.S. Cheng, H.C. Yeh, G.M. Kanapilly, Am. Ind. Hygiene J. 42 (1981) 605–610.

[18] D. Lee, A. Miller, D.B. Kittelson, M.R. Zachariah, J. Aerosol Sci. 37 (1) (2005) 88–110.

[19] H.G. Wagner, in: D. Siegla, G. Smith (Eds.), Proceedings of International Symposium on Particulate Carbon Formation During Combustion, General Motors Research Lab, 1980, pp. 1–28.

[20] K. Siegmann, K. Sattler, H.C. Siegmann, J. Electron Spectrosc. Relat. Phenom. 126 (2002) 191–202.

[21] D.M. Roessler, F.R. Faxvog, R. Stevenson, G.W. Smith, in: D. Siegla, G. Smith (Eds.), Proceedings of International Symposium on Particulate Carbon Formation During Combustion, General Motors Research Lab, 1980, pp. 57–84.

[22] M.J. Pipho, D.B. Kittelson, L. Luo, D. Zarling, Tech. Paper 921646, Society of Automotive Engineers, 1992, pp. 111–126.

[23] M.A. Barris, S.B. Reinhart, F.H. Wahlquist, Tech. Paper 910131, Society of Automotive Engineers, 1991, pp. 19–28.

[24] P.A. Bonczyk, Combust. Flame 87 (1991) 233–244.
[25] K.E. Ritrievi, J.P. Longwell, A.F. Sarofim, Combust. Flame 70 (1987) 17–31.
[26] T. Hirasawa, C.J. Sung, Z. Yang, A. Joshi, H. Wang, Combust. Flame 139 (2004) 288–299.
[27] N. Miyamoto, H. Zhixin, A. Harada, H. Ogawa, T. Murayama, Paper 871612, Society of Automotive Engineers, 1997, pp. 1–7.